Journal of Power Sources 195 (2010) 7829–7837

Contents lists available at ScienceDirect

Journal of Power Sources

journal homepage: www.elsevier.com/locate/jpowsour

Analysis of a fuel cell hybrid commuter railway vehicle

Danushka Meegahawatte[a], Stuart Hillmansen[a,*], Clive Roberts[a], Marco Falco[a], Andrew McGordon[b], Paul Jennings[b]

[a] Birmingham Centre for Rail Research and Education, University of Birmingham, Birmingham B15 2TT, United Kingdom
[b] Warwick Manufacturing Group, International Manufacturing Centre, University of Warwick, Coventry CV4 7AL, United Kingdom

ARTICLE INFO

Article history:
Received 1 October 2009
Received in revised form 25 January 2010
Accepted 1 February 2010
Available online 25 February 2010

Keywords:
Fuel cell
Railway
Hybrid
Hydrogen
Supervisory controller
Battery

ABSTRACT

This study presents paper presents an analysis of the potential CO_2 savings that could be gained through the introduction of hydrogen-powered fuel cells on a commuter-style railway route. Vehicle is modelled as a fuel cell series hybrid. The analysis consists of power/energy flow models of a fuel cell stack, battery pack and hybrid drive controller. The models are implemented in a custom C# application and are capable of providing key parametric information of the simulated journey and individual energy drive components. A typical commuter return journey between Stratford Upon Avon and Birmingham is investigated. The fuel cell stack and battery pack behaviour is assessed for different stack sizes, battery sizes and control strategies to evaluate the performance of the overall system with the aim of understanding the optimum component configuration. Finally, the fuel (H_2) requirements are compared with typical diesel and hybrid-diesel powered vehicles with the aim of understanding the potential energy savings gained from such a fuel cell hybrid vehicle.

1. Introduction

Railway transport is arguably one of the least environmentally damaging forms of transport [1]. Widely deployed electrification means that the majority of passenger kilometres generate zero emissions at the point of use. Railways also share in the CO_2 benefits that occur through increasing de-carbonization of grid electricity. On the other hand, the extremities of most railway networks contain lightly-loaded routes that are uneconomic to electrify [2]. The vehicles that operate on these routes are currently diesel powered, and therefore are exposed to future fuel supply issues and uncertain future costs. In the short- to medium-term, these vehicles could be replaced or re-engineered to utilize hybrid propulsion systems, with a view to replace eventually the diesel prime mover with a fuel cell when reliability can be proven and an economic case can be made.

Hybrid devices produce near-zero emissions at the point of use. Today, much research is taking place into the use of fuel cells, which can range in output power from a few to several thousand kilowatts, in transport applications such as automobiles, buses, locomotives, ships, and submarines. Many different types of fuel cell are now available and in transport sectors the most popular is the proton exchange membrane (PEM) based technology. PEM fuel cells (PEMFCs) offer a valid alternative for transportation vehicles [3] and the literature contains some analysis of fuel cell locomotives in applications such as tunneling, mining [4] and hybrid shunt locomotives [5]. The existing analysis [6,7] provides a suitable foundation on which to develop this investigation.

As fuel cells run on hydrogen as opposed to fossil fuels such as coal, petroleum, and natural gas they have the potential of being a carbon-neutral source of energy. At present, the challenge is the efficient extraction and delivery of hydrogen. There are many technologies available to obtain hydrogen, of which the most popular is the steam reforming of natural gas. Currently, this is the most energy-efficient and large-scale method of hydrogen production [8–10], but CO_2 is produced in this process:

$$CH_4 + 2H_2O + \text{Energy} \rightarrow 4H_2 + CO_2 \quad (1)$$

The simplest carbon-neutral method of obtaining H_2 is by electrolysis of water:

$$H_2O + \text{Energy} \rightarrow H_2 + \frac{1}{2}O_2 \quad (2)$$

If the electrical energy for this process is obtained from renewable sources (i.e., hydropower, solar energy or wind energy) it is possible to produce hydrogen with no impact on greenhouse gases [11].

In this study, paper the effects of a hybrid energy propulsion drive on a commuter rail vehicle are investigated. The behaviour of the fuel cell stack and battery pack is assessed for different stack sizes, battery sizes and control strategies to evaluate the

* Corresponding author.
E-mail address: s.hillmansen@bham.ac.uk (S. Hillmansen).

0378-7753/$ – see front matter © 2010 Elsevier B.V. All rights reserved.
doi:10.1016/j.jpowsour.2010.02.025

Table 1
Journey details (Stratford Upon Avon to Birmingham Moore Street).

Start location	Stratford Upon Avon Station
End location	Stratford Upon Avon Station (via Birmingham Moore Street Station)
Stations	34
Station list	Stratford Upon Avon, Wilmcote, Wootton Wawen, Henley in Arden, Danzey, Wood End, The Lakes, Earlswood, Wythall, Whitlocks End, Shirley, Yardley Wood, Hall Green, Spring Road, Tyseley, Small Heath, Bordesley, Birmingham Moore Street (and back)
Journey length	78.58 km

performance of the overall system with the aim of understanding the optimum component configuration. Finally, the fuel (H_2) requirements are compared with a typical diesel and hybrid-diesel powered vehicles with the aim of understanding the potential energy and CO_2 savings gained from such a fuel cell hybrid vehicle.

2. Journey details

All results reported in this investigation are centred around a Class 150 Diesel Multiple Unit (DMU) railway vehicle running along a segment of the Birmingham Snow Hill Line in the United Kingdom between Stratford Upon Avon and Birmingham Moore Street Station. Details of the selected journey and vehicle are given in Tables 1, 2 and Fig. 1(a) and (b).

3. Railway vehicle simulation

The basic forces that govern the behaviour of a railway vehicle are shown in Fig. 2. The vehicle response is achieved by solving the equation of motion by using Lomonossoff's equation [12]:

$$M_e \frac{d^2 s}{dt^2} = F - R - Mg \sin\alpha \tag{3}$$

where M is the total mass of the vehicle; M_e is the inertial mass of the vehicle; g is the gravitational acceleration; R is the resistance to motion the vehicle experiences while moving along the track; $\sin\alpha$ is the gradient of the track; F is the total tractive effort produced at the powered wheels of the vehicle; s is the vehicle displacement.

The term R is the resistance to motion encountered by the vehicle (apart from gravity). This is made up of the sum of mechanical friction, frictional losses due to the vehicle interacting with the running rails, and aerodynamic drag. With help from the following Davis Equation, the total resistance to motion (R_t) can be expressed empirically as:

$$R_t = A + B\frac{ds}{dt} + C\left(\frac{ds}{dt}\right)^2 + D\frac{Mg}{r} + Mg\alpha \tag{4}$$

where ds/dt is the velocity of the vehicle; r is the radius of track curvature; α is the gradient angle of the track ($\sin\alpha \approx \alpha$, where, $\alpha \to 0$); A, B, C and D are constants.

Table 2
Vehicle characteristics for a Class 150 DMU.

Railway vehicle	British Rail, Class 150 DMU
Mass	76.5×10^3 kg
Number of seats	124
Speed (max)	33.5 m s^{-1} ($\approx$ 75 mph)
Tractive effort (max)	$\approx$ 40.0 kN
Tractive power (max; at wheels)	374 kN
Base speed	8 m s^{-1} ($\approx$ 18 mph)
Percentage of powered axles	50%
Acceleration mass coefficient (λ)	0.08
Davis equation coefficients	$A = 2.09 \times 10^3$ N $B = 9.83$ N m^{-1} s $C = 6.51$ N m^{-2} s^2 $D = 0.00$ kg^{-1}

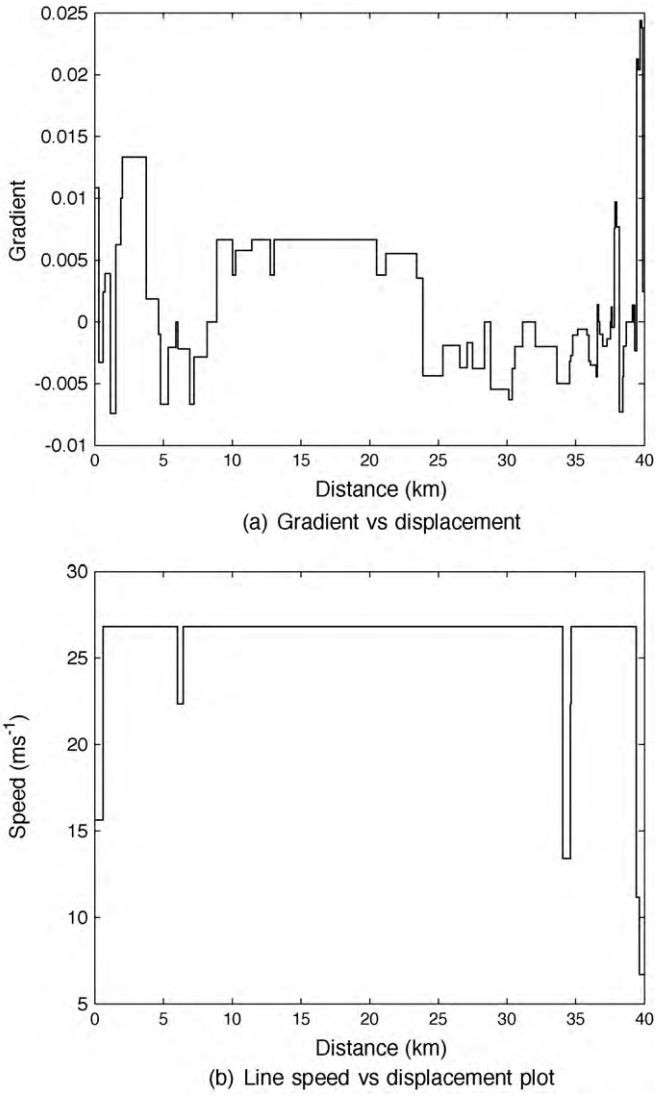

Fig. 1. (a and b) Details of simulated route between Stratford upon Avon to Birmingham Moore Street.

The vehicle response can be calculated for a given track and vehicle characteristic by solving the following equation:

$$M_e \frac{d^2 s}{dt^2} = TE - \left[A + B\frac{ds}{dt} + C\left(\frac{ds}{dt}\right)^2 + D\frac{Mg}{r} + Mg\alpha\right] \tag{5}$$

where TE is the total tractive effort delivered by the powered wheels; A, B, C and D can be determined by vehicle characteristic data obtained by run-down tests or by the use of the

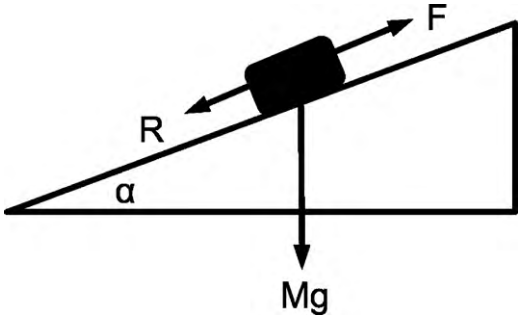

Fig. 2. Forces acting upon a typical railway vehicle.

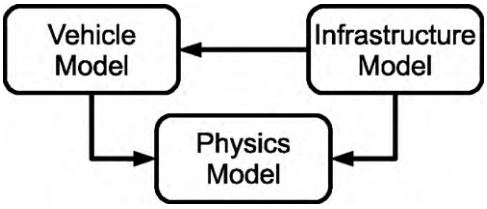

Fig. 3. Railway vehicle simulator function block.

methods proposed by Armstrong and Swift [13] for UK rolling stock.

3.1. Vehicle simulator

The vehicle simulator implemented in this work consists of three fundamental components:

- infrastructure model,
- vehicle model,
- physics model.

The Infrastructure Model provides all spatial and temporal information about the simulated railway journey. This includes the characteristics of the track, signalling information such as line speeds, and station stops along the route (Fig. 3).

The function of the **Vehicle Model** is to control the behaviour of the vehicle as it moves along the track. This is achieved by adjusting the output tractive effort based on the vehicle traction effort curves and geographic and signalling information from the Infrastructure Model. This is implemented by a combination of comparing the current line speed, next line speed, and the distance to the next station (see Fig. 4).

Finally, the actual vehicle response is calculated by the **Physics Model** with the aid of Eq. (5). The vehicle speed and displacement values are calculated by using numerical integration.

4. Hybrid energy propulsion drive

The tractive power for the railway simulation outlined in Section 3.1 is derived from a hybrid energy propulsion drive model based on a series hybrid architecture (Fig. 5) and consists of the following models:

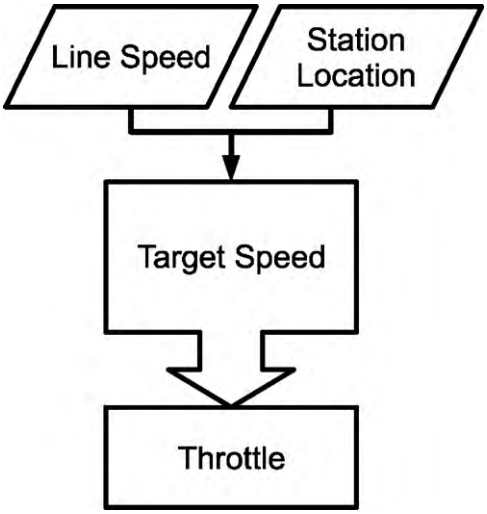

Fig. 4. Driving strategy evaluator function block.

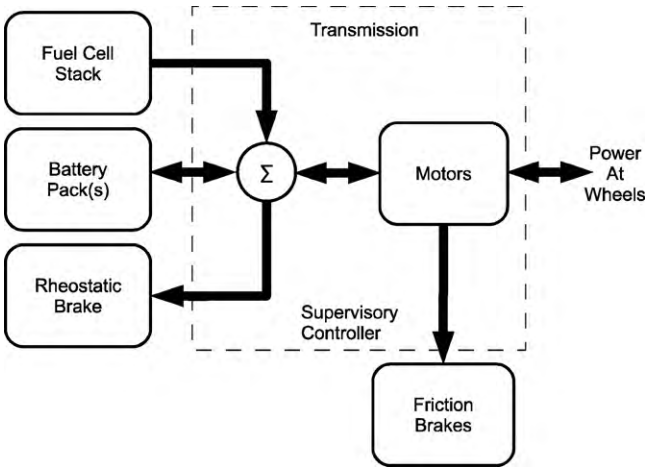

Fig. 5. Hybrid energy drive.

- fuel cell stack,
- battery pack,
- rheostatic brake,
- hybrid controller.

The total power output from the hybrid energy propulsion drive can be obtained from Eq. (6).

$$P_{total}(t) = P_{FC}(t) + P_{Battery}(t) + P_{EB}(t) \quad (6)$$

where $P_{total}(t)$ is the total power output of the hybrid energy propulsion drive; $P_{FC}(t)$, $P_{Battery}(t)$ and $P_{EB}(t)$ are the power output from the fuel cell, battery pack and rheostatic brake, respectively. It should be noted that these values are dependent on the model parameters and vary with the state of each model and vehicle behaviour over the course of the simulation.

4.1. Fuel cell model

For the purpose of this work, a PEMFC was chosen to be modeled. In order to operate the stack at its optimum efficiency, the fuel flowing into the stack must change according to the output power of the fuel cell stack. In practice, however, the response of a fuel cell system is constrained by the response times of the external pumps, compressors and control loops that govern the overall system [14]. Therefore, the operational efficiency of a typical fuel cell system is adversely effected by transient output power demands. This is primarily due to the relationship between stack power and the fuel flowing through the cells at any given moment.

The properties of the modelled fuel cell stack are presented in Table 3. It should be noted that the model is in essence a static model of a fuel cell system. For the purpose of this work, to obtain a better match between the response of the model and the application, the following assumptions and constraints were enforced on the model.

- The model output power relates to the total output power flowing to the transmission (in the case of a series hybrid architecture, the

Table 3
Fuel cell model parameters.

Type	Proton exchange membrane
Voltage at P_{max}	0.41 V
n_{cells}	800
U_{H_2}	1.0
M_H	1.00794 g mol^{-1}

Table 4
Fuel cell power limits.

FC ID	Power max (kW h)	Positive gradient (kW s^{-1})	Negative gradient (kW s^{-1})
1	470	15.7	50.0
2	570	19.0	50.0
3	670	22.3	50.0
4	770	25.7	50.0
5	870	29.0	50.0

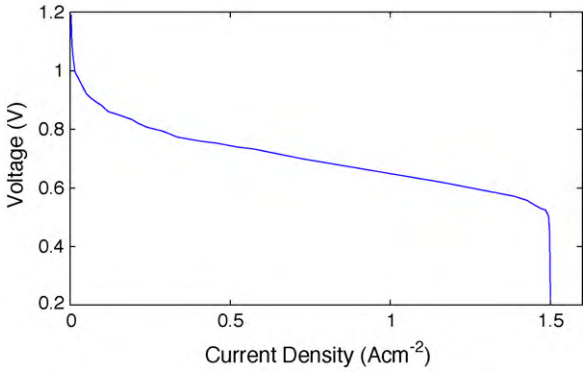

Fig. 6. Fuel cell voltage vs. current density.

d.c. link) of the hybrid energy propulsion drive (thus including the d.c.–d.c. converter, fuel cell stack, and all its sub-systems).
- The output power of the overall fuel cell model cannot be altered instantaneously. Instead, an increase or decrease in output power is limited by a predetermined rate of change of power (Table 4).
- In all cases, the time taken for the fuel cell system to reach its maximum output power is approximately 30 s.
- The above-mentioned maximum power of the fuel cell stack is obtained by varying the active area of the cells within the stack.
- A voltage–current density curve (Fig. 6) is used to determine the cell output voltage.
- The output power of the fuel cell stack is determined by a power-efficiency curve [15] (Fig. 7).
- The fuel consumption (in this case H_2) is obtained with the aid of Eqs. (7) and (8) [16].

$$q_{H_2} = \frac{M_{H_2} I_{FC}}{nF} \tag{7}$$

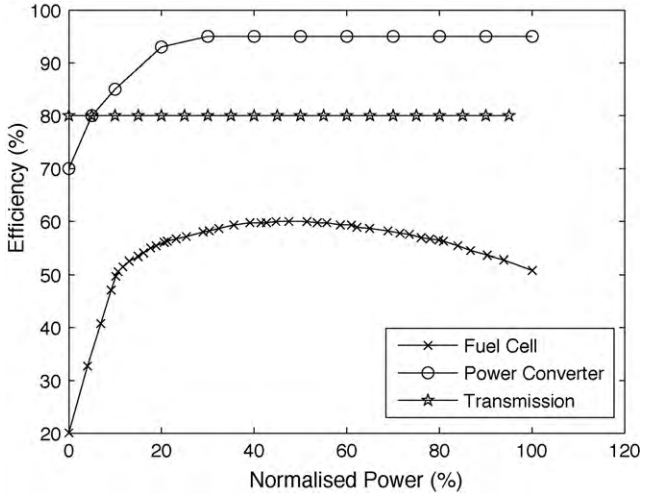

Fig. 7. Normalised output power vs. efficiency for fuel cell stack, power converter of battery pack and transmission/motors.

Table 5
Battery model configuration.

Type	NiCd
Pack OC voltage	300 V
Capacity per pack	100 Ah
Initial *SOC*	50%
SOC_{min}	20%
SOC_{max}	80%
SOC_{topup}	30%

$$F_{H_2} = \frac{n_{cells}}{U_{H_2}} \int q_{H_2} \cdot dt \tag{8}$$

where q_{H_2} is the hydrogen consumption rate; M_{H_2} is the molar mass of H_2; n is the number of electrons involved; I_{FC} is the current flowing through the stack; F is the Faraday constant (96,450 C mol^{-1}); F_{H_2} is the total hydrogen consumed; n_{cells} is the total number of cells in the stack; U_{H_2} is the utilisation ratio of hydrogen.

4.2. Battery pack model

For the purpose of this work, a battery capacity model was developed based on a 300 V, 100 Ah, nickel–cadmium battery pack [17]. The properties of the simulated battery pack are presented in Table 5. Furthermore, the following assumptions and constraints are applied to the operation of the battery pack.

- The model output relates to the output power at the d.c. link of the hybrid energy drive.
- The output power of the overall system cannot be altered instantaneously. Instead an increase or decrease in output power is limited by a predetermined rate of change of power (Table 6).
- The state-of-charge (SOC) of the battery pack is calculated with the aid of Eq. (11). The efficiency of the battery pack is affected by the efficiency-power response curve of the d.c.–d.c. converter (Fig. 7).

$$P_{Battery} = \frac{P_{out}}{\mu_{\Delta t}} \tag{9}$$

$$\Delta SOC = \frac{\Delta E_{\Delta t}}{E_{total}} = \frac{P_{Battery} \Delta t}{VC} \tag{10}$$

$$SOC = SOC_{initial} + \int \Delta SOC \cdot dt \tag{11}$$

where ΔSOC is the change in SOC; $\Delta E_{\Delta t}$ is the change in energy in unit time Δt; E_{total} is the total energy capacity of battery; $P_{Battery}$ is the power flow; Δt is the time step; V is the voltage of the pack and C is the combined capacity (Ah) of the battery packs; P_{out} is the output power of the complete battery system (including power converters); $\mu_{\Delta t}$ is efficiency.

4.3. Rheostatic brake model

For the purpose of this work, a rheostatic brake model was developed. The function of the 'Rheostatic Brake' was to absorb any excess energy that the battery pack model could not accept (e.g., during fully-charged states). The relative amount of energy

Table 6
Battery power limits.

	Providing power (discharging)	Accepting power (charging)
Positive gradient (MW s^{-1})	1.0	1.0
Negative gradient (MW s^{-1})	1.0	1.0
Maximum power (kW)	500.0	500.0

Table 7
Rheostatic brake model configuration.

Type	Rheostatic brake
Maximum power	500.0 kW

absorbed by the rheostatic brake model is therefore dependent on the operational characteristics of the battery pack model.

The following assumptions and constraints have been made in the modelling.

- The brake can absorb any power demand up to a predetermined limit (Table 7).
- The brake can dissipate the accepted power with no performance limitations for any period of time (i.e., the performance of brakes does not degrade with prolonged use).

4.4. Hybrid controller model

The dynamic behaviour of the components is achieved by means of power flow modelling of the above sub-systems. Two control strategies were implemented and simulated in this work [18]:

- **LL-CS** is a Load Levelling Control Strategy where primary power for propulsion is supplied by the fuel cell system, while the battery pack is used to supplement the peak power demand and absorb braking energy.
- **TC-CS** is a Trickle Charge Control Strategy where the battery pack provides the primary power for the vehicle propulsion while absorbing the braking energy. The fuel cell stack operates at its optimum efficiency when the hybrid energy drive is accelerating, maintaining vehicle speed or stationary (e.g., idling at station). When vehicle deceleration is taking place, the stack is switched off.

The above control strategies are used only while the state-of-charge of the battery pack remains within its safe operating limits of SOC_{min} and SOC_{max} (Table 5). Should the SOC drop below the preset threshold, SOC_{topup}, the controller will attempt to top-up the battery pack charge via the fuel cell stack with a charging power equal to the battery pack capacity (i.e., 30 kW power charge for a battery pack of 30 kWh capacity). In this state, the propulsion power is sourced from the fuel cell stack. Once the battery pack reaches 50% SOC, the selected control strategy operation resumes.

In the event that the battery reaches the upper limit of the allowed state-of-charge (SOC_{max}), the controller switches off the fuel cell stack and draws power for propulsion only from the battery pack until its SOC reaches 50% at which point the selected control strategy operation resumes. In any of the above cases, if the battery pack is not capable of absorbing the required energy (i.e., while regenerative braking) then the excess energy is dissipated via the rheostatic brake.

5. Results and discussion

5.1. Simulator validation

Fig. 8 is the vehicle speed vs. displacement plot of a class 150 DMU travelling along half of the selected route. The three plots represent the measured results (dashed line) obtained via a handheld Global Positioning System (GPS) receiver placed in the vehicle, simulated data (solid line), and line speed (dotted line). It should be noted that the measured journey differs slightly from the journey described in Section 2, due to the vehicle not stopping at all the stations. This is due to some stations along the route being request stops. It should be noted that the mass of the vehicle has been assumed to be constant for each type of propulsion system, and therefore the required power and performance of each vehicle type are similar. It is estimated that the different mass of each propulsion system would have negligible effect on the total vehicle mass, and therefore is an important, but second-order effect. This issue would merit further investigation in more depth.

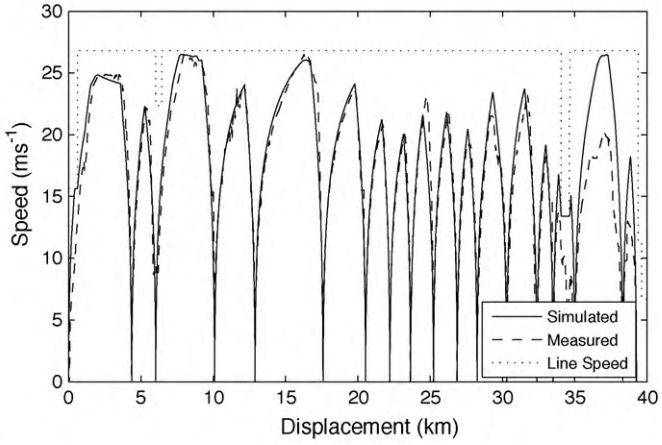

Fig. 8. Vehicle speed, line speed vs. displacement (Stratford upon avon to Birmingham Moore Street).

Table 8
Diesel multiple unit results.

Fuel consumption	102 l
Journey duration	5711 s
Powering energy	294.4 kWh
Braking energy	124.8 kWh

5.2. Diesel multiple unit analysis

A vehicle powered by a 500 kW diesel engine for primary motive power is simulated [19]. The engines of the vehicle are operated along the traditional propeller curve, and give a total fuel consumption of 102 l (Table 8). If the CO_2 emissions for a diesel vehicle is 2.73 kg l^{-1} [20], the total CO_2 produced is 278.5 kg.

5.3. Diesel hybrid analysis

A vehicle based on the diesel vehicle described in Section 5.2 with an additional battery pack was used. The vehicle is operated in electric-only mode, i.e., with the diesel engines turned off until the power demanded reaches a level where the engine can operate efficiently. At higher speeds, the vehicle operates with both electrical and diesel power, with the operation of the engine being constrained around its optimum operating point. The vehicle captures the kinetic energy and stores it in the battery under braking. The total fuel consumption for this vehicle and journey is 82 l (Table 9), with the SOC at the end of the journey being within 2% of the starting value. This relates to 224 kg of CO_2 for the journey.

Table 9
Diesel hybrid results.

Fuel consumption	82 l
Journey duration	5711 s
Powering energy	294.4 kWh
Braking energy	124.8 kWh

Table 10
Pure fuel cell results.

Hydrogen consumption	38.0 kg
Journey duration	6275.1 s
Powering energy	355.0 kWh
Braking energy	96.6 kWh

5.4. Pure fuel cell analysis

A fuel cell vehicle with a 470 kW stack is used to provide motive power for the vehicle. The fuel cell only vehicle is found to take approximately 10 min longer (Table 10) than the diesel vehicle to complete the given journey. This is primarily due to the reduced rate of change of power (dp/dt) in the fuel cell stack compared to the modeled diesel vehicle. The lower acceleration caused by the reduced rate of change of power prevents the vehicle by reaching the target line speed for a significant proportion of the journey therefore reduces the available energy to be recovered via regenerative braking.

The total hydrogen consumption obtained by the simulation provides a means of benchmarking any fuel cell hybrid vehicle configurations to determine any energy savings.

5.5. Fuel cell hybrid analysis

To determine the optimum configuration of the control strategy, fuel cell and battery to achieve the best possible performance for a hybrid drivetrain a design method based on a simple trial and error was chosen. The method consists of evaluating different hybrid drivetrain configurations and control strategies to obtain an optimum configuration capable of servicing the intended application.

In this work, the five fuel cell stack configurations listed in Table 4 were evaluated with five battery packs that had capacities ranging from 100 to 500 Ah in 100 Ah steps. The resulting 25 hybrid energy drive combinations were used to power the railway vehicle simulator described in Section 3. The control strategies described in Section 4.4 were used to govern each hybrid power plant. The results from the simulations are presented in Figs. 9 and 10 and Tables 11 and 12.

Table 11
Fuel cell hybrid results for load leveling control strategy.

FC ID	Pack count				
	*x*1	*x*2	*x*3	*x*4	*x*5
(a) Mean state of charge (%)					
1	31.862	31.143	34.781	35.521	34.117
2	38.083	30.950	33.011	43.847	47.188
3	45.766	49.326	53.431	55.683	55.555
4	54.289	57.994	57.683	60.673	61.276
5	59.585	58.122	59.801	60.288	62.133
(b) Hydrogen consumption (kg)					
1	33.597	32.629	31.47	32.134	31.105
2	30.201	29.343	28.173	27.328	27.324
3	28.643	27.826	27.646	27.643	27.643
4	27.358	26.866	25.851	25.518	27.946
5	26.889	26.106	26.259	25.143	24.593
(c) Total journey duration (s)					
1	6040.0	5948.3	5859.4	5831.2	5783.6
2	5882.1	5835.5	5765.3	5729.3	5729.2
3	5780.1	5733.5	5729.5	5729.2	5729.2
4	5771.1	5734.1	5729.3	5729.1	5729.2
5	5774.6	5736.1	5729.4	5729.0	5729.0
(d)Total rheostatic braking energy (kWh)					
1	0.06	1.37	1.91	2.52	1.67
2	0.06	0.05	0.07	0.09	0.09
3	0.06	0.07	0.08	0.08	0.08
4	2.59	0.08	0.12	0.14	0.08
5	3.76	0.14	0.11	0.15	0.16

Table 12
Fuel cell hybrid results for trickle charge control strategy.

FC ID	Pack count				
	*x*1	*x*2	*x*3	*x*4	*x*5
(a) Mean state of charge (%)					
1	34.211	34.435	41.079	40.802	39.517
2	52.379	49.684	26.202	47.665	50.604
3	54.241	56.596	57.666	59.16	58.93
4	61.504	62.19	61.992	61.676	63.179
5	62.26	63.025	62.814	63.633	62.844
(b) Hydrogen consumption (kg)					
1	29.087	31.23	28.11	27.642	27.645
2	28.645	28.719	28.307	27.059	27.040
3	28.852	28.291	27.216	28.194	27.443
4	30.092	30.152	27.436	28.358	26.388
5	32.033	30.807	28.787	27.805	28.991
(c) Total journey duration (s)					
1	5971.8	5914.6	5814.4	5796.7	5795.7
2	5810.4	5785.1	5747.0	5729.4	5729.3
3	5800.3	5736.8	5729.6	5729.3	5729.3
4	5854.4	5738.0	5729.4	5729.3	5729.3
5	5895.4	5739.0	5729.3	5729.3	5729.3
(d) Total rheostatic braking energy (kWh)					
1	1.238	2.442	2.315	2.787	3.217
2	2.986	1.523	0.994	0.753	0.747
3	4.252	0.697	0.766	0.767	0.765
4	6.264	0.762	0.779	0.784	0.799
5	8.261	0.833	0.824	0.835	0.879

5.5.1. Load-levelling control strategy

All simulation runs start with a battery SOC of 50%, as shown in Fig. 9(e). The final SOC varies significantly while the mean SOC over the journey ranges from 31 to 62%, i.e., a variation of over 30%. The highlighted SOC profiles correspond to the three main modes in which the hybrid controller operates, i.e.,

- **A** – shows a configuration that requires the controller to intervene because the battery SOC reaches the upper allowed limit (SOC_{max}).
- **B** – is when intervention is required due to the battery SOC reaching a critically low (SOC_{topup}) level.
- **C** – outlines a profile in which the selected control strategy is utilized for the duration of the journey with no intervention.

In a charge-sustaining hybrid power plant for stable and sustainable operation, the mean SOC must ideally be close to the initial value. Very small swings in SOC often correspond to a battery pack that is over-sized, thereby adding unnecessary weight and cost to the system. Conversely, large SOC swings, particularly ones that reach the permitted upper or lower limits, correspond to a battery pack that is too small for the hybrid configuration. Furthermore, in these configurations the adopted control strategy becomes ineffective as the supervisory controller must intervene when the SOC of the storage device is outside the safe operating limits.

Table 13
Comparion of CO_2 emissions by power plant type.

Power plant type	CO_2 emissions		
	Total (kg)	Grams per seat km	kg per vehicle km
Diesel	278.5	27.9	3.54
Diesel hybrid	224.0	22.4	2.85
Fuel cell	209.0	20.9	2.69
FC hybrid	148.5	14.8	1.88

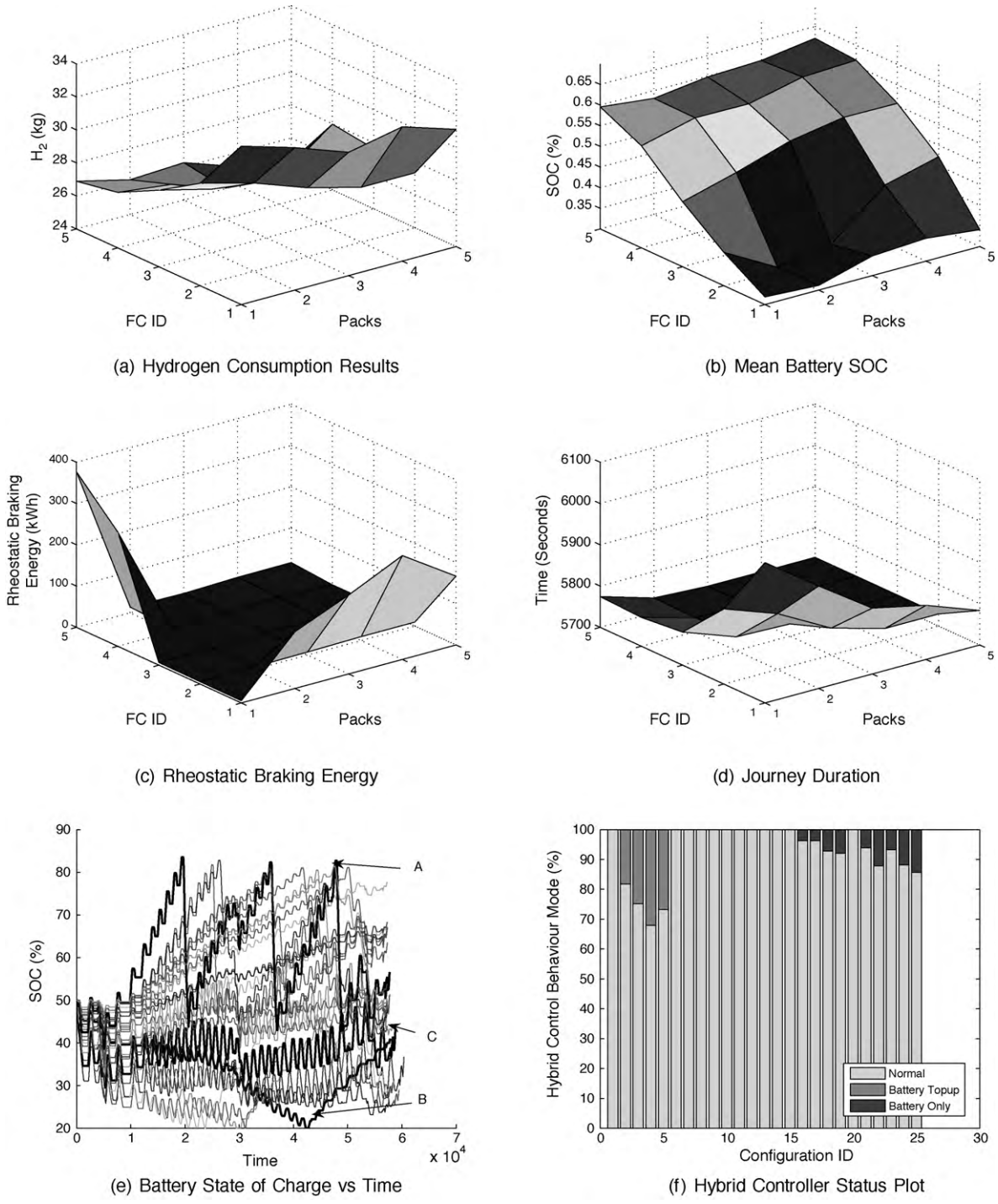

Fig. 9. (a–f) Fuel cell hybrid results for load leveling control strategy.

It can be deduced that with this control strategy for configurations which utilize smaller fuel cell stacks, the battery often needs an top-up charge; whereas for the configurations with larger fuel cell stacks, the battery has a tendency to be over charged and requires continuous discharging to remain within the operating limits, as shown by Fig. 9(f). The selected control strategy plays the most significant role for configurations that utilize a fuel cell stack of 570 and 670 kW irrespective of battery pack capacity.

A significant proportion of energy is lost via rheostatic braking instead of being captured by the battery pack in configurations with the smallest battery pack capacities, as illustrated by Fig. 9(c). This is due mostly to the smaller packs not being able to absorb large amounts of energy in the relatively short period of time during which the vehicle is decelerating. Somewhat high amounts of energy are lost for configurations that use the smallest fuel cell stack (470 kWh). This is because the hybrid controller spends a significant proportion of time topping up the battery charge due to the battery SOC dropping below the lowest permissible limit (Fig. 9(f)). During this charging period, hybrid operation is suspended and therefore braking energy must be dissipated via the rheostatic brake.

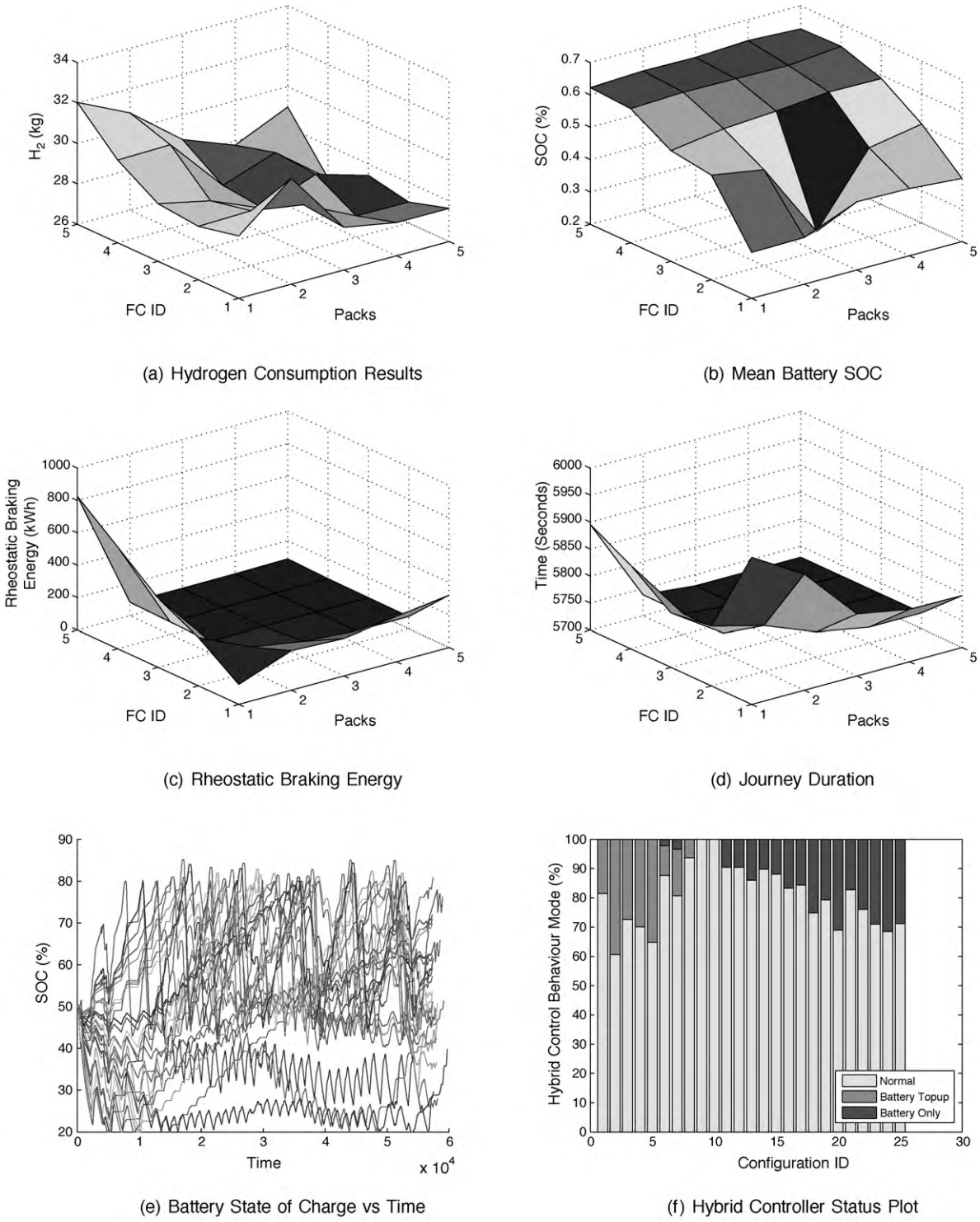

Fig. 10. (a–f) Fuel cell hybrid results for trickle charge control strategy.

Finally, the total journey duration does not change significantly over the different configurations (by approximately 5 min) but the overall consumption of hydrogen varies between 24.5 and 33.5 kg, i.e., a variation of 9 kg.

5.5.2. Trickle charge control strategy

The battery SOC is prone to drift significantly outside the safe operating levels (Fig. 10(f)), due to the large proportion of time the hybrid control strategy operation is suspended on account of the SOC reaching its limits and the supervisory controller intervening. The rheostatic braking energy content plot shows that, in accord with the load-levelling control strategy, a significant amount of energy is lost for the smallest battery pack and smallest fuel cell stack power configurations. The causes of these results are similar in nature to the previous results.

The variation in overall journey duration is approximately 4 min (Fig. 10(d)). This is most likely due to the significant intervention by the hybrid controller to maintain the battery SOC, especially with configurations that utilize larger battery packs and/or fuel cell stacks.

There is a 5 kg difference in hydrogen consumption between the best and worst fuel economies, but the relatively low variation is likely to be due to the control strategy not being used for large portions of the journey in many of the configurations.

6. Discussion and concluding remarks

The relationship between H_2 generation and CO_2 emissions varies significantly and is largely based on the method by which the hydrogen is produced. Currently, steam reforming of natural gas comprises almost 50% of the world production of hydrogen. If hydrogen is obtained by means of stream reforming, approximately 5.5 kg of CO_2 is generated for every 1 kg of H_2[8]. If hydrogen is obtained by electrolysis of water using electricity from traditional power plants, this figure will increase further, namely, 62 kWh of energy (currently from mostly non-renewable sources) is needed to create 1 kg of hydrogen. This figure can be reduced to zero by the de-carbonization of electricity grids via the use of renewable energy, such as solar or wind power, and carbon capture and storage programs. These technologies, however, are not yet feasible for the large scale of production that would be necessary to power an entire fleet of fuel cell railway vehicles. Therefore, for the scope of this work, it is assumed that hydrogen will be generated via the steam reforming of methane (Table 13).

Analysis of the above results shows that the most suitable configuration is a 670 kW fuel cell stack with 60–90 kWh of energy storage and utilizing a load-levelling control strategy. This provides a hydrogen consumption of 27 kg for the simulated journey. This amount translates to approximately 148.5 kg of CO_2. It should be noted that the emission will be higher in practice as the calculation does not take into account indirect CO_2 contributors in the conversion process such as electricity that is obtained by mostly fossil-fuel powered power plants.

Compared with a pure fuel cell vehicle, a hybridized fuel cell vehicle provides nearly a 30% reduction in fuel and emissions, while not significantly effecting the overall journey duration (increase of less than 2%). Compared with a pure diesel vehicle, fuel cell hybrid vehicles have the potential of reducing CO_2 emissions by up to 45%. Analysis of the two control strategies presented in this work show that the optimum performance of a hybrid drivetrain is significantly affected by the adopted hybrid control strategy. The study has concentrated on a typical UK commuter railway journey, and consideration should be made of adaptability of the optimum architectures to other typical routes.

References

[1] A. Schafer, Transport. Res. A: Policy Pract. 32 (6) (1998) 455–477.
[2] B. Destraz, P. Barrade, A. Rufer, in: PESC 04: 2004 IEEE 35th Annual Power Electronics Specialists Conference, vols. 1–6, Conference Proceedings, IEEE Power Electronics Specialists Conference Records, Aachen, Germany, June 20–25, 2004, pp. 677–682.
[3] J. Amphlett, R. Mann, B. Peppley, P. Roberge, A. Rodrigues, in: Proceedings of the Tenth Annual Battery Conference on Applications and Advances, 1995, pp. 221–226.
[4] M. Betournay, G. Desrivieres, P. Laliberte, M. Laflamme, A. Miller, D. Barnes, CIM Bull. 96 (1074) (2003) 72–76.
[5] F. Donnelly, R. Cousineau, R. Horsley, in: Proceedings of the 2004 ASME/IEEE Joint Rail Conference, Baltimore, MD, April 06-08, 2004, pp. 113–117.
[6] A.R. Miller, J. Peters, in: Proceedings of the 2006 Joint Rail Conference on Restoring and Upgrading Rail Infrastructure, Rolling Stock and Systems, Vol. 31 of ASME RTD, Atlanta, GA, April 04–06, 2006, pp. 287–293.
[7] K. Runtz, M. Lyster, in: Canadian Conference on Electrical and Computer Engineering, 2005, pp. 794–797.
[8] A. Haryanto, S. Fernando, N. Murali, S. Adhikari, Energy Fuels 19 (5) (2005) 2098–2106, doi:10.1021/ef0500538.
[9] D. Das, T. Veziroglu, Int. J. Hydrogen Energy 26 (1) (2001) 13–28.
[10] R.B. Duffey, Int. J. Energy Res. 33 (2, Sp. Iss. SI) (2009) 126–134; in: 3rd International Energy, Energy and Environment Symposium (IEEES-3), Evora, Portugal, July 01–05, 2007, doi:10.1002/er.1428.
[11] S.I. Allakhverdiev, V.D. Kreslavski, V. Thavasi, S.K. Zharmukhamedov, V.V. Klimov, T. Nagata, H. Nishihara, S. Ramakrishna, Photochem. Photobiol. Sci. 8 (2) (2009) 148–156, doi:10.1039/b814932a.
[12] R. Hill, Power Eng. J. 8 (1) (1994) 47–56.
[13] B. Rochard, F. Schmid, Proc. Inst. Mech. Eng. F: J. Rail Rapid Transit 214 (4) (2000) 185–199.
[14] W. Yang, B. Bates, N. Fletcher, R. Pow, Control challenges and methodologies in fuel cell vehicle development, SAE Paper 98C054.
[15] K. Jeong, B. Oh, J. Power Sources 105 (1) (2002) 58–65.
[16] F. Barbir, T. Gamez, Int. J. Hydrogen Energy 22 (10–11) (1997) 1027–1037.
[17] D. Brown, M. Alexander, D. Brunner, S.G. Advani, A.K. Prasad, J. Power Sources 183 (1) (2008) 275–281, doi:10.1016/j.jpowsour.2008.04.089.
[18] Modelling of Alternative Propulsion Concepts of Railway Vehicles, The Modelica Association, 2006.
[19] S. Hillmansen, C. Roberts, Proc. Inst. Mech. Eng. F: J. Rail Rapid Transit 221 (1) (2007) 135–143, doi:10.1243/09544097JRRT99.
[20] Emission facts – average carbon dioxide emissions resulting from gasoline and diesel fuel (February 2005), doi:EPA420-F-05-001. http://www.epa.gov/oms/climate/420f05001.pdf.